Carbon 128 (2018) 78–85

Contents lists available at ScienceDirect

Carbon

journal homepage: www.elsevier.com/locate/carbon

Carbon dots with red-shifted photoluminescence by fluorine doping for optical bio-imaging

Wanning Yang [a, 1], Hong Zhang [b, 1], Junxin Lai [b], Xinyi Peng [a], Yuping Hu [b], Wei Gu [b, *], Ling Ye [b, **]

[a] School of Basic Medical Sciences, Capital Medical University, Beijing, 100069, PR China
[b] School of Pharmaceutical Sciences, Capital Medical University, Beijing, 100069, PR China

ARTICLE INFO

Article history:
Received 30 September 2017
Received in revised form
19 November 2017
Accepted 23 November 2017
Available online 23 November 2017

ABSTRACT

Carbon dots (CDs) are environmentally benign alternatives to quantum dots comprised of heavy metals with outstanding photoluminescent (PL) properties and have shown great promise in optical bio-imaging and sensing. However, it remains challenging to rationally design and synthesize CDs with red PL emission. We herein disclose that a red-shifted PL emission could be achieved by doping the electron-withdrawing fluorine atoms into CDs. Moreover, we demonstrate the preparation of fluorine doped CDs with a red PL emission under excitation at 530 nm by an easy, environmental friendly, one-step microwave-assistant carbonation route. A possible mechanism of the red-shifted emission upon fluorine doping is tentatively proposed. In addition, the applicable of these red-emissive fluorine doped CDs as optical nanoprobes for bio-imaging applications, both *in vivo* and *in vitro*, was explored. It is indicated that the as-prepared fluorine doped CDs with red-shifted PL emission are promising candidates for tumor bio-imaging/or diagnostics.

1. Introduction

Carbon-based nanomaterials have received significant attention because of their remarkable properties and potential use in a variety of applications [1–3]. Fluorescent carbon dots (CDs), as a new member in this fascinating family, have shown great promise in bio-imaging and optical sensing by virtue of their outstanding photoluminescent (PL) properties, such as high photo-stability and lack of photo-blinking [4–12]. Another extraordinary aspect of CDs that has attracted considerable attention is the cost-effective and environment-friendly synthesis and excellent biocompatibility, which can hardly be realized with conventional semiconductor quantum dots [13]. These benefits allow CDs to be readily incorporated into biological systems for bio-related applications.

To date, the most common CDs exhibit PL from blue to green while only a few CDs possess PL emission in longer-wavelength regions [14–17] and it remains challenging to rationally design and synthesize CDs with the desired PL properties (e.g. red PL emission), most likely due to a lack of sufficient theoretical and experimental knowledge on the origin of PL in CDs. Nonetheless, there is mounting evidence that the PL emission of CDs originates from both an intrinsic band gap resulting from isolated sp^2 conjugation in the core of CDs and a surface state that can be either directly excited or excited by energy transfer from an intrinsic band [18]. As a consequent, a desirable PL emission of CDs could be achieved either by modifying the surface functional groups and/or by controlling the domain size of sp^2 conjugation.

The surface defects (e.g. oxygen-containing functional groups) serve as capturing centers of excitons and lead to the surface-state-related PL [19]. Increased surface defects by oxidation would narrow the energy levels and consequently cause the red-shifted PL emission of CDs [20–22]. In contrast, blue-shifted PL emission of CDs can be achieved by surface reduction [23]. On the other hand, the band gap of isolated sp^2 domains within the CDs core could function as PL centers as well and the size of sp^2 conjugated fragments determines the band gaps (quantum size effects) [24]. As the size of the fragment increases, the gap gradually decreases and results in a red-shifted PL of CDs [25,26]. Alternatively, incorporation of heteroatoms to the CDs core is another effective strategy to control the PL of CDs. For example, the doping of nitrogen atoms

* Corresponding author.
** Corresponding author.
E-mail addresses: weigu@ccmu.edu.cn (W. Gu), lingye@ccmu.edu.cn (L. Ye).
[1] These authors contributed equally to this work.

https://doi.org/10.1016/j.carbon.2017.11.069
0008-6223/

into CDs results in a red-shifted PL emission [27–30], which is due to the electron-doping effect of the doped graphitic nitrogen atoms.

It is well documented that introduction of electron-withdrawing fluorine atoms in polyconjugated systems could result in a red-shifted fluorescence [31–33]. Inspired by this, we postulate that introduction of fluorine atoms in addition of nitrogen atoms on the sp^2 conjugated domains in the CDs core might be an effective strategy for further increasing the extent of red-shift. To testify this, we prepared fluorine and nitrogen co-doped CDs through an easy, environmental friendly, one-step microwave synthesis route using citric acid as the carbon source, urea as the nitrogen dopant, and sodium fluoride as the fluorine dopant. These fluorine doped CDs show a red-shifted PL emission compared to that of the CDs without fluorine doping, resulting a red PL under excitation at 530 nm. A possible mechanism is tentatively proposed to explain the behavior of red-shift upon fluorine doping. Moreover, the applicable of these red emissive CDs as optical nanoprobe for bio-imaging was testified, both *in vivo* and *in vitro*.

2. Experimental

2.1. Chemicals

Citric acid, urea, and sodium fluoride were purchased from Sinopharm Chemical Reagent Co., Ltd. (Beijing, China). 3-(4,5-Dimethylthiazolyl-2)-2,5-diphenyltetrazolium bromide (MTT) cell proliferation assay kit was purchased from Amresco. Fetal bovine serum (FBS) and Dulbecco's modified Eagle's medium (DMEM) were provided by Gibco (Basel, Switzerland). All other chemicals were of analytical grade and used as received. Double distilled water was used throughout the experiments.

2.2. Synthesis of CDs

A one-step microwave-assisted method was adapted with minor modifications to prepare CDs [34]. Briefly, 180 mg of citric acid, 540 mg of urea and 100 mg of sodium fluoride were added in 10 mL water. The mixture was sonicated and then heated in a domestic microwave oven (750 W, Galanz, China) for 5 min. The obtained CDs were re-dispersed in water and purified by the dialysis against double distilled water using a Spectra/Por dialysis membrane (MWCO = 100–500 Da) for 24 h. Finally, a clear dark yellowish aqueous dispersion containing CDs was obtained for further use.

2.3. Characterization

The morphology and size of CDs were observed by a JEM-2100 F transmission electron microscopy (TEM, JEOL, Japan) at operating voltage of 200 kV. For TEM imaging, one drop of aqueous suspension of the CDs was deposited on a carbon-coated copper grid and dried under vacuum. The size distribution profile of CDs was acquired on a Nano-ZS90 Zetasizer (Malvern, UK). The X-ray diffraction (XRD) pattern of CDs-was obtained on a PANalytical X'pert Pro MPD diffractometer (PANalytical, Holland), using Cu Kα radiation ($\lambda = 1.5405$ Å) at a voltage of 40 kV and a current of 40 mA with 2θ scanning mode. The Fourier-transform infrared (FTIR) spectrum of CDs with a resolution of 4 cm^{-1} was collected over the range of 600–4000 cm^{-1} on an ATR diamond-crystal-equipped miniature FTIR spectrometer (Nicolet iS5 FT-IR spectrometer and iD5 ATR accessory). XPS analysis was performed on an axis ultra-spectrometer (Kratos, UK) using mono-Al Kα line (1486.71 eV) radiation. The UV absorption spectra of CDs were recorded on a UV-3010 spectrophotometer (Hitachi, Japan) using a 1 cm path length cuvette. The room temperature PL emission spectra together with the quantum yield (QY) of CDs were measured on an FLS-980 fluorescence spectrophotometer (Edinburgh Instruments, UK) equipped with an integrating sphere.

2.4. Cytotoxicity assay

C6 glioma cells were seeded in a 96-well plate at 1×10^4 per well and cultured in DMEM medium in a humidified 5% CO_2 incubator at 37 °C for 24 h. Then, the cells were treated with CDs at different concentrations (0, 0.1, 0.2, 0.3, 0.4, 0.5, 0.6 mg mL^{-1}). After incubation for 24 h, the medium was refreshed and 20 μL of MTT (5 mg mL^{-1}) was added, followed by incubating for 4 h to allow formation of formazan dye. Next, the medium was discarded and DMSO was added into each well. The optical density (OD) value was measured on a Multiskan microplate spectrophotometer (Thermo Fisher Scientific, USA) at a wavelength of 490 nm. The cell viability was assessed by the ratio of OD values between the experimental and control group and was expressed as mean ± standard deviation which deviations from three independent experiments.

2.5. Histopathological examination

Healthy ICR mice were injected with 200 μL of the CDs at a dosage of 20 mg kg^{-1} or with saline as the control. Seven days after injection, the major tissues (heart, liver, spleen, kidneys, lung and brain) were harvested and fixed in 10% formalin solution. The histopathological tests were performed according to standard procedures. In brief, the tissue samples were embedded in paraffin blocks and sectioned into 5 μm slices, followed by hematoxylin and eosin (H&E) staining. The stained sections were observed on an optical microscope (Leica DM4000B) at 10 × magnification.

2.6. In vitro cell imaging

After being seeded on the cover slips at a density of 2×10^4 cells, the glioma C6 cells were cultured in DMEM supplemented with 10% of FBS under humidified 5% CO_2 condition at 37 °C for 12 h. The culture medium was then replaced with FBS-free DMEM containing CDs (0.5 mg mL^{-1}) and the cells were incubated for another 12 h. The cell imaging was performed on a confocal laser scanning microscope (CLSM) with an excitation of 530 nm (Leica TSC SP5).

2.7. In vivo imaging

All animal experiments were performed according to protocols evaluated and approved by the ethical committee of Capital Medical University. Xenograft tumor was established by subcutaneous injection of a suspension of 2×10^6 C6 cells in PBS (60 μL) into the right flanks of male nude mouse (4-week-old, 15–20 g) and was allowed to grow for 8–10 d till the tumor size reached approximately 6 mm. CDs (0.2 mg mL^{-1}, 200 μL) were then intravenously injected into the tumor-bearing nude mouse. The fluorescent imaging were performed at various time points (1, 5, 10, 20, 40, 60, 90 min and 12 h post-injection) on a Kodak *in vivo* FX Pro imaging System (Kodak, USA) using a 530 nm excitation light and a 600 nm emission filter.

3. Results and discussion

3.1. Characterizations

The morphology and size of CDs were examined on the TEM image (Fig. 1a). It was found that the CDs appear as well-separated semi-spherical dots with a size of approximate 10 nm. Fig. 1b shows the high resolution TEM (HRTEM) image of CDs. Note that the CDs exhibits identical well-resolved lattice fringes with a spacing of

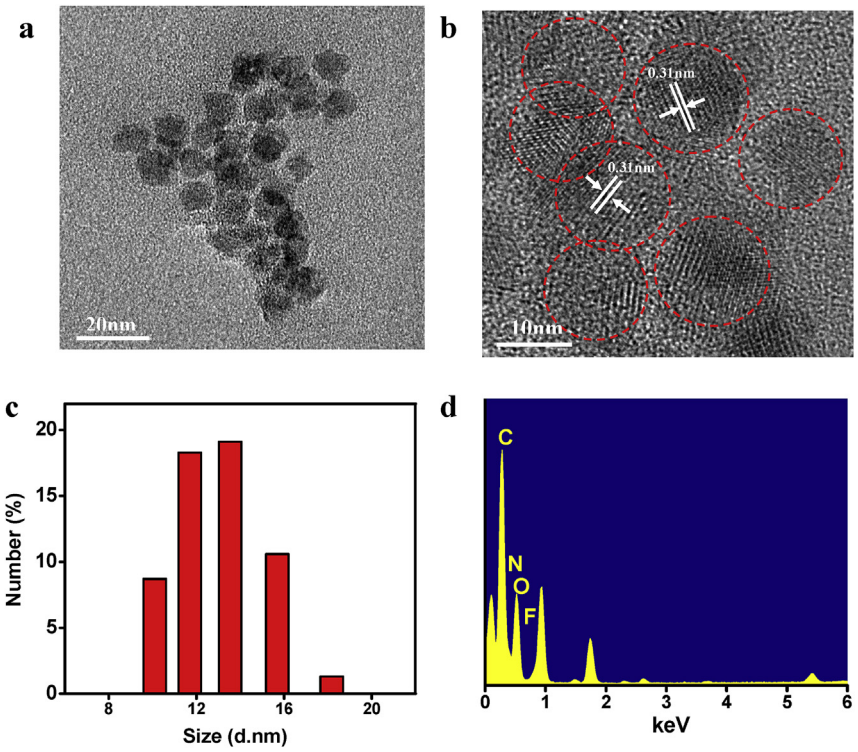

Fig. 1. TEM (a) and HRTEM (b) images, size distribution(c), and EDS spectrum (d) of the CDs. (A colour version of this figure can be viewed online.)

0.31 nm, which is in agreement with the 002 plane of graphitic carbon and indicates the high crystallinity of CDs. The size of CDs is consistent with the size distribution determined by DLS (Fig. 1c). Moreover, the presence of fluorine in the CDs is confirmed by the energy dispersive spectrometry (EDS) analysis (Fig. 1d).

The crystalline nature of CDs was further identified by XRD. As presented in Fig. 2a, the broad reflection in the XRD pattern corresponds to typically amorphous carbonaceous materials while the sharp diffraction peak at 27.4° represents the characteristic interplanar stacking of aromatic systems that indexes to the 002 facet of graphite [35]. However, compared to the ordered crystal structure of graphite, the slightly upward shift (from 26.5° to 27.4°) indicates disordered carbon and decrease in the sp^2 layers spacing in the carbonization process. Based on the TEM and XRD, it can be deduced that the CDs consist of high crystalline domains within the carbon core and amorphous regions on the surfaces.

Furthermore, the surface functional groups and the composition of CDs were probed by IR. The IR spectrum of the CDs shown in Fig. 2b suggests the presence of abundant oxygen containing functional groups on their surfaces; such groups include hydroxyl (ν_{O-H}, 3428 cm^{-1}), carboxyl ($\nu_{C=O}$, 1743 cm^{-1}), and carbonyl ($\nu_{C=O}$, 1630 cm^{-1}) groups. Moreover, stretching vibrations of C=C (1524 cm^{-1}), C=N (1642 cm^{-1}), C–N= (1427 cm^{-1}), and N–H (3200 cm^{-1}) bonds are observed, indicating the formation of hetero-polyaromatic structures in the CDs during the carbonization process [28]. The surface functional groups and the composition of CDs were additionally identified by XPS. As shown in Fig. 2C, the XPS C1s spectrum consists of four deconvoluted Gaussian distributions at 284.6, 286.3, 288.39, and 290.84 eV, which can be assigned to C–C (sp^3), C–N (sp^3), C=O (sp^2), and O–C=O (sp^2), respectively. Meanwhile, the XPS O1s spectrum is dominated by one peak at 531.28 eV originated from C=O and the N1s peak at 399.58 eV indicates that most nitrogen is in the C–N form. Moreover, the presence of fluorine in CDs is supported by the XPS F1s spectrum and the shift of C=O and O–C=O peaks to higher binding energy observed in the XPS C1s spectrum.

3.2. PL properties

The presence of surface oxygen-containing groups makes CDs well water-dispersible. Moreover, the hybridization between these surface functional groups and the carbon core renders the CDs distinct PL behaviors. Fig. 3 illustrated the PL emission contour maps of CDs with or without fluorine doping when excited from 520 to 550 nm. As can be seen, both CDs exhibit excitation-dependent PL emission phenomenon. Note that the dependence of emission wavelength on excitation wavelength has been identified as a generic feature of most CDs, suggesting that CDs might possess multiple PL centers resulting from either different conjugation length of the carbon core or various surface functional groups. Nevertheless, the fluorine doping led to a red-shifted PL with respect to the CDs without fluorine doping. Consequently, when excited at 530 nm, the fluorine doped CDs emit red PL, while the CDs without fluorine doping appears yellowish green under excitation at 530 nm (Inset, Fig. 3). Previous study shows that the self-assembled aggregation, which occurs at high concentration, could lead to a red-shifted emission of CDs [36]. To eliminate such effect, the absorbance of both CDs was kept below 0.1 at 530 nm. In addition, the corresponding fluorescence images were obtained on the *in vivo* fluorescence imaging system using a 530 nm excitation light and a 600 nm emission filter. Obviously, the fluorine doped CDs show much intensive red fluorescence signal (Fig. S1). The QY of fluorine doped CDs upon excited at 530 nm, however, is about 1.2% as measured directly by the integrating sphere, which demands continued efforts to further improve their QY.

3.3. Mechanism of red-shifted emission

Generally, the emission wavelength of PL materials is related to the energy gap between excited states and the ground state, while

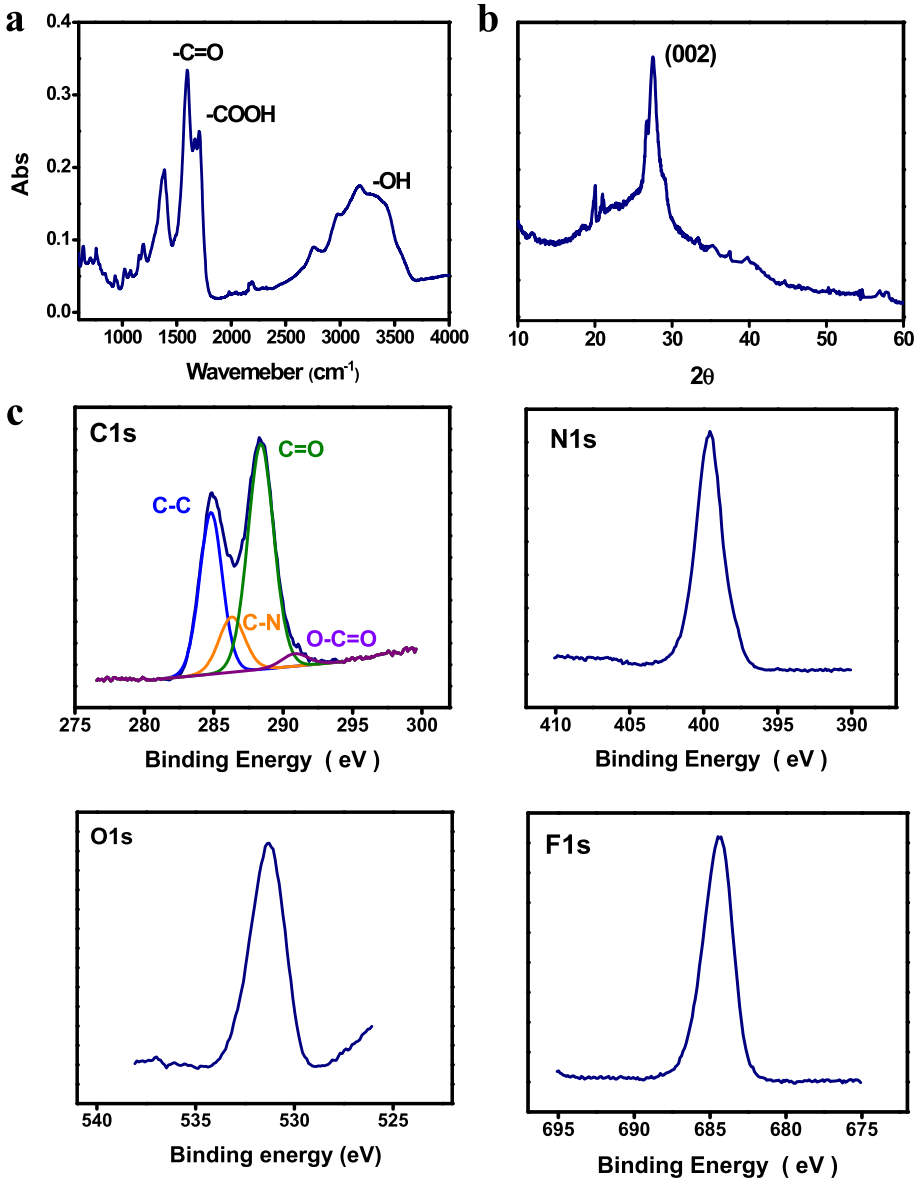

Fig. 2. (a) XRD pattern, (b) IR spectrum and (c) XPS C1s, N1s, O1s, and F1s spectra of the CDs. (A colour version of this figure can be viewed online.)

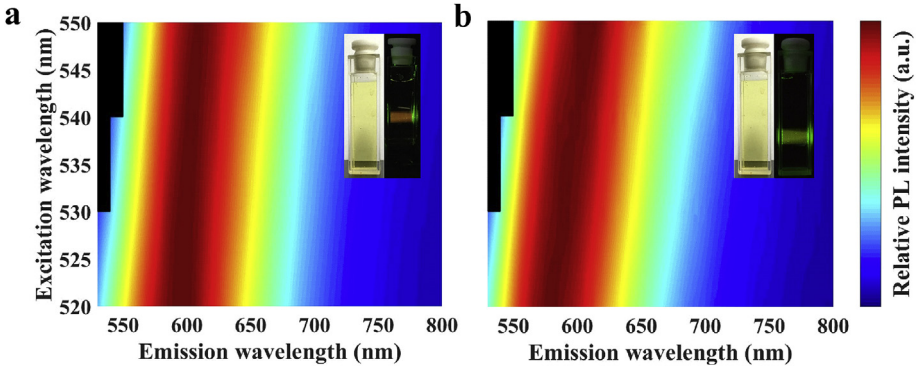

Fig. 3. PL emission contour maps of CDs under different excitations from 520 to 550 nm. Insets show the pictures of CDs with or without fluorine doping under daylight and upon excited at 530 nm. (A colour version of this figure can be viewed online.)

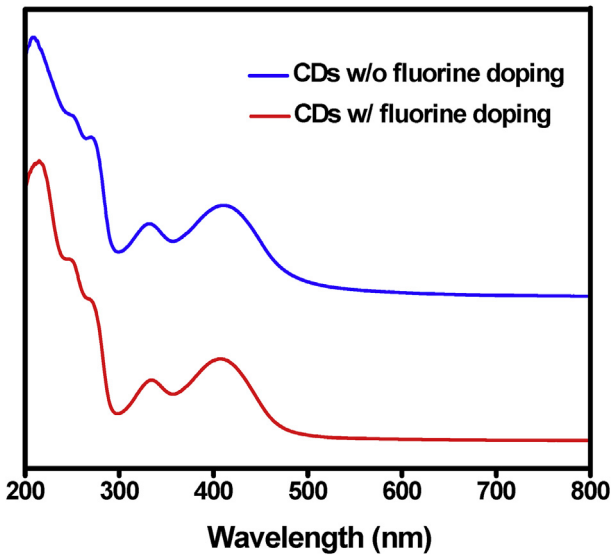

Fig. 4. UV–vis absorption spectra of CDs with and without fluorine doping. (A colour version of this figure can be viewed online.)

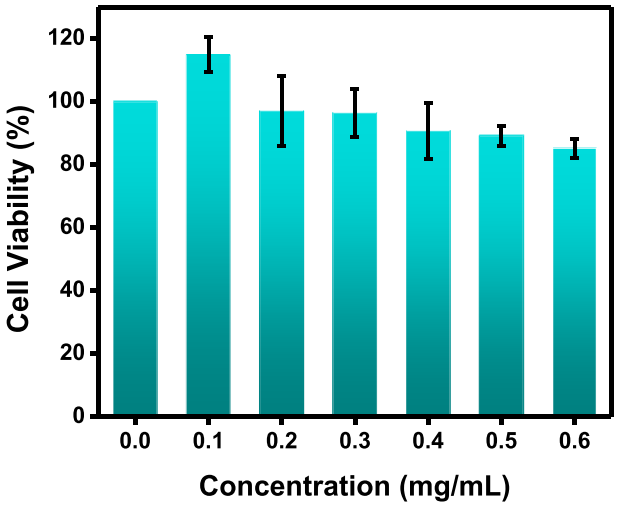

Fig. 6. Viability of C6 cells treated with the CDs at various concentrations. (A colour version of this figure can be viewed online.)

energy levels of the electronic states are dominated by the intrinsic electronic structure of the materials [37]. The UV–vis absorption spectra of CDs with or without fluorine doped were collected. As shown in Fig. 4, the feature of absorption spectra of both CDs is similar. For example, both show bands at 340 and 410 nm attributing to the n–π^* transition of C=O bonds from different surface oxygen-containing functional groups and the bands at 255 and 282 nm corresponding to the π–π^* transitions of C=C and C=N bonds in the carbon core, respectively, which was formed after dehydration between the hydroxyl, carboxyl, and amino groups from citric acid and urea, as well as subsequent carbonization process during the preparation of CDs. Nevertheless, the UV–vis absorbance band for the π–π^* transition at ~220 nm is different for CDs with or without fluorine doping. For fluorine doped CDs, this band is red-shifted with relatively high absorbance, implying an extended π-electron system in the carbon core. It has been shown that the π-electron system can strongly couple with surface electronic states and alters the overall electronic structure of the CDs [37]. In light of the UV–Vis absorbance and the aforementioned XPS results, we speculate that the change in the extent of the π-electron system due to the fluorine doping is responsible for the red-shifted PL emission of CDs, that is, an increase in the extent of the π-electron system would narrow the energy gap of the π–π^* transitions and further result in a small energy gap for the surface states [38]. This consequently lowers the energy levels and causes the red-shifted PL emission (Fig. 5). Nevertheless, the underlying mechanism of red-shifted PL upon fluorine doping awaits further investigations.

3.4. Toxicity

The unique red-emissive PL of the fluorine doped CDs suggests the potential for bio-imaging. Nevertheless, the toxicity is a crucial concern for bio-related applications. Therefore, the toxicity of CDs was examined prior to cellular and *in vivo* imaging applications. Firstly, the toxicity of CDs towards cells was tested by the standard cell viability MTT assay. After incubation with the CDs at different concentrations for 24 h, the cell viability was determined and the result is plotted in Fig. 6. As can be seen, the cell viability decrease slight with the increasing of CDs concentration. Nevertheless, the viability of C6 cells remains higher than 80% at all testing concentrations, verifying the cytobiocompatibility of CDs.

Furthermore, the *in vivo* toxicity of CDs was evaluated by histological analyzing the H&E stained tissue slices from mice administered with CDs. Compared with the control groups, no obvious inflammation, cell necrosis, or apoptosis are observed in

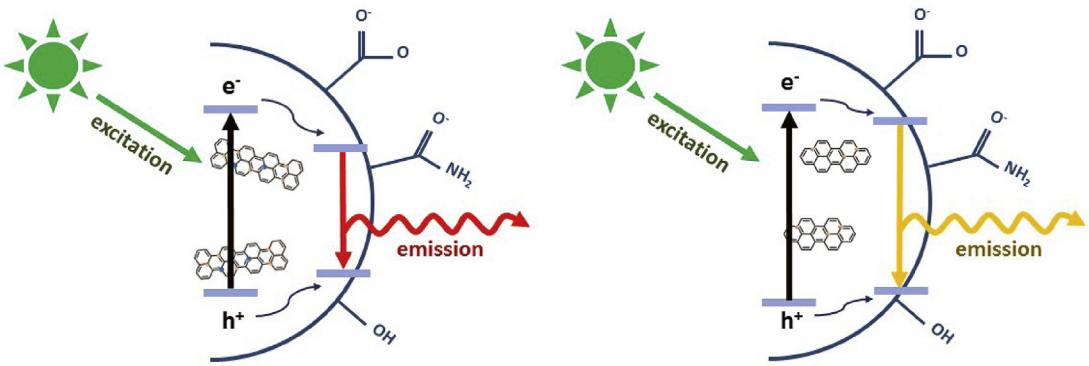

Fig. 5. Schematic representation of mechanism for red-shifted PL emission upon fluorine doping. An increase in the extent of the π-electron system due to the fluorine doping narrows the energy gap of the π–π^* transitions and result in a small energy gap for the surface states. (A colour version of this figure can be viewed online.)

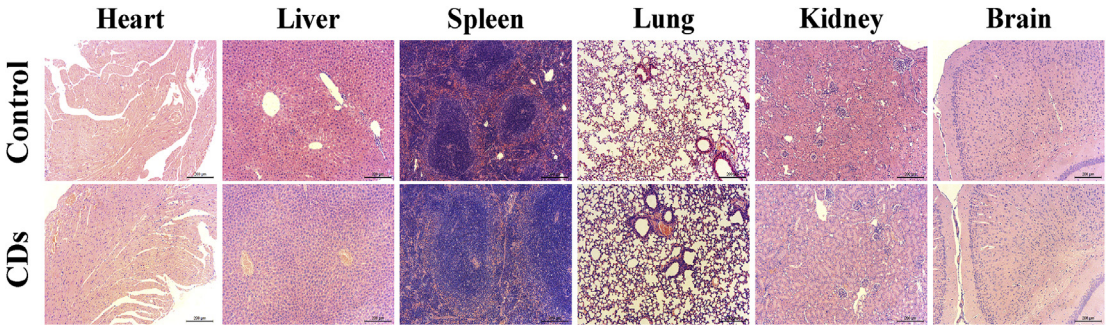

Fig. 7. H&E stained slices of heart, liver, spleen, lung, kidney and brain harvested from the mice receiving saline (the control) or the CDs. (A colour version of this figure can be viewed online.)

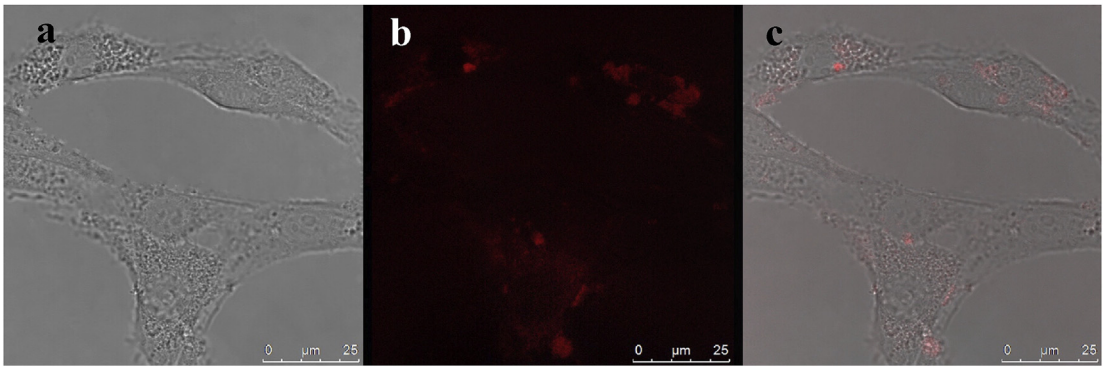

Fig. 8. CLSM images of C6 cells treated with CDs under bright field (a), under excitation at 530 nm (b) and overlay of a and b (c). (A colour version of this figure can be viewed online.)

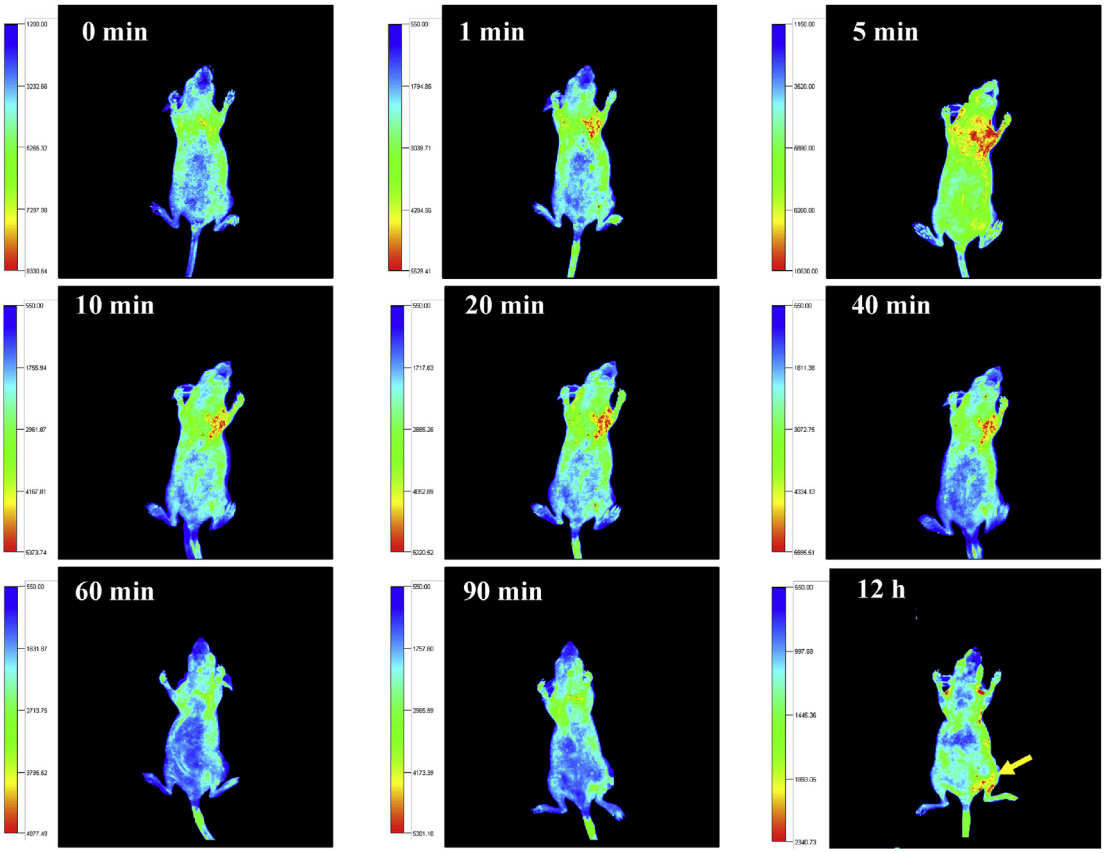

Fig. 9. *In vivo* fluorescent images of nude mouse bearing xenograft tumor before and after i.v. injection of CDs at different time points. (A colour version of this figure can be viewed online.)

the major organs including heart, liver, spleen, lung, kidney, and brain (Fig. 7), implying the good biocompatibility of CDs.

3.5. *In vitro* and *in vivo* bio-imaging

The red PL emission excited with a longer visible light source could result in less adverse effects on cells and tissues. Moreover, red PL emission enables a deeper penetration, which is beneficial for *in vivo* bio-imaging. In this context, the unique red-emissive PL and good biocompatibility suggests the suitability of these fluorine doped CDs for bio-imaging applications. To testify this, *in vitro* cell imaging was first conducted by CLSM. After incubation of the CDs at a concentration of 0.5 mg mL^{-1} for 6 h, the C6 cells emit red fluorescence in the cytoplasm under excitation at 530 nm (Fig. 8), suggest that the CDs could be efficiently internalized by CDs. The CLSM result clearly verifies the potential of CDs for optical bio-imaging at cellular level. Moreover, no substantial change in morphology is observed for C6 cells treated with the CDs, which further confirms the low cytotoxicity of CDs.

Additionally, the feasibility of CDs for *in vivo* bio-imaging was explored on xenograft tumor bearing nude mouse using a Kodak *in vivo* fluorescence imaging system with a 530 nm excitation light and a 600 nm emission filter. Fig. 9 shows the fluorescent images of the tumor-bearing nude mouse acquired before and after intravenously injected of the CDs solution (200 μL, 2 mg mL^{-1}) at different time points. An intensive fluorescence signals are initially observed in the lung area, suggesting that the injected CDs underwent a blood circulation. After 12 h of circulation, fluorescence signal mainly locates in the tumor area, indicating that the CDs could efficiently accumulate in the tumor as a result of the enhanced permeability and retention (EPR) effect. Moreover, the mouse remained healthy after the injections, further demonstrating the biocompatibility of CDs. Therefore, the red-emissive fluorine doped CDs could be used as promising optical nanoprobes for tumor detection and diagnostics at both cellular and whole-body level.

4. Conclusion

In sum, we disclose for the first time that the fluorine doping leads to an increased extent of π-electron system in the CDs core and consequently red-shifts the PL emission. As a proof of concept, the CDs with red PL under excitation at 530 nm were prepared by fluorine doping. These fluorine doped CDs are biocompatible, as verified by *in vitro* MTT assay and *in vivo* H&E histological analysis. Moreover, the *in vitro* cell imaging and *in vivo* fluorescence imaging of tumor-bearing mouse demonstrate the potential of fluorine doped, red-emissive CDs as optical nanoprobes in bio-imaging. The results of this study add piece of new insight to the PL mechanism of CDs and provide an effective strategy for preparation CDs with red-shifted PL.

Acknowledgements

The authors gratefully acknowledge the financial supports from the Key Project from Beijing Commission of Education (KZ201610025022), Beijing Natural Science Foundation (7162023), and National Natural Science Foundation of China (81271639). The technical supports from the Core Facility Center (CFC) at Capital University of Medical are greatly acknowledged.

Appendix A. Supplementary data

Supplementary data related to this article can be found at https://doi.org/10.1016/j.carbon.2017.11.069.

References

[1] V. Georgakilas, J.A. Perman, J. Tucek, R. Zboril, Broad family of carbon nanoallotropes: classification, chemistry, and applications of fullerenes, carbon dots, nanotubes, graphene, nanodiamonds, and combined superstructures, Chem. Rev. 115 (2015) 4744–4822.
[2] U.N. Maiti, W.J. Lee, J.M. Lee, Y. Oh, J.Y. Kim, J.E. Kim, et al., Chemically modified/doped carbon nanotubes & graphene for optimized Nanostructures & Nanodevices, Adv. Mater. 26 (2014) 40–67.
[3] H. Gong, R. Peng, Z. Liu, Carbon nanotubes for biomedical imaging: the recent advances, Adv. Drug Deliv. Rev. 65 (2013) 1951–1963.
[4] S.N. Baker, G.A. Baker, Luminescent carbon nanodots: emergent nanolights, Angew. Chem. Int. Ed. 49 (2010) 6726–6744.
[5] Y.P. Sun, B. Zhou, Y. Lin, W. Wang, K.A.S. Fernando, P. Pathak, et al., Quantum-sized carbon dots for bright and colorful photoluminescence, J. Am. Chem. Soc. 128 (2006) 7756–7757.
[6] S.-T. Yang, L. Cao, P.G. Luo, F. Lu, X. Wang, H. Wang, et al., Carbon dots for optical imaging in vivo, J. Am. Chem. Soc. 131 (2009) 11308–11309.
[7] L. Cao, X. Wang, M.J. Meziani, F. Lu, H. Wang, P.G. Luo, et al., Carbon dots for multiphoton bioimaging, J. Am. Chem. Soc. 129 (2007) 11318–11319.
[8] K. Hola, Y. Zhang, Y. Wang, E.P. Giannelis, R. Zboril, A.L. Rogach, Carbon dots-Emerging light emitters for bioimaging, cancer therapy and optoelectronics, Nano Today 9 (2014) 590–603.
[9] S.Y. Lim, W. Shen, Z. Gao, Carbon quantum dots and their applications, Chem. Soc. Rev. 44 (2015) 362–381.
[10] F. Ostadhossein, D. Pan, Functional carbon nanodots for multiscale imaging and therapy, Wiley Interdiscip. Rev. Nanomed Nanobiotechnol 9 (2017), e1436.
[11] H. Li, Z. Kang, Y. Liu, S.-T. Lee, Carbon nanodots: synthesis, properties and applications, J. Mater Chem. 22 (2012) 24230–24253.
[12] L. Zhou, F. Wu, J. Yu, Q. Deng, F. Zhang, G. Wang, Titanium carbide (Ti_3C_2Tx) MXene: a novel precursor to amphiphilic carbide-derived graphene quantum dots for fluorescent ink, light-emitting composite and bioimaging, Carbon 118 (2017) 50–57.
[13] J.-H. Liu, S.-T. Yang, X.-X. Chen, H. Wang, Fluorescent carbon dots and nanodiamonds for biological imaging: preparation, application, pharmacokinetics and toxicity, Curr. Drug Metab. 13 (2012) 1046–1056.
[14] J. Ge, Q. Jia, W. Liu, L. Guo, Q. Liu, M. Lan, et al., Red-emissive carbon dots for fluorescent, photoacoustic, and thermal theranostics in living mice, Adv. Mater. 27 (2015) 4169–4177.
[15] S. Sun, L. Zhang, K. Jiang, A. Wu, H. Lin, Toward high-efficient red emissive carbon dots: facile preparation, unique properties, and applications as multifunctional theranostic agents, Chem. Mater. 28 (2016) 8659–8668.
[16] K. Jiang, S. Sun, L. Zhang, Y. Lu, A. Wu, C. Cai, et al., Red, green, and blue luminescence by carbon dots: full-color emission tuning and multicolor cellular imaging, Angew. Chem. Int. Ed. 54 (2015) 5360–5363.
[17] M. Shamsipur, A. Barati, S. Karami, Long-wavelength, multicolor, and white-light emitting carbon-based dots: achievements made, challenges remaining, and applications, Carbon 124 (2017) 429–472.
[18] S. Zhu, Y. Song, X. Zhao, J. Shao, J. Zhang, B. Yang, The photoluminescence mechanism in carbon dots (graphene quantum dots, carbon nanodots, and polymer dots): current state and future perspective, Nano Res. 8 (2015) 355–381.
[19] S.K. Das, Y. Liu, S. Yeom, D.Y. Kim, C.I. Richards, Single-particle fluorescence intensity fluctuations of carbon nanodots, Nano Lett. 14 (2014) 620–625.
[20] L. Bao, C. Liu, Z.-L. Zhang, D.-W. Pang, Photoluminescence-tunable carbon nanodots: surface-state energy-gap tuning, Adv. Mater. 27 (2015) 1663–1667.
[21] H. Ding, S.-B. Yu, J.-S. Wei, H.-M. Xiong, Full-color light-emitting carbon dots with a surface-state-controlled luminescence mechanism, ACS Nano 10 (2016) 484–491.
[22] L. Bao, Z.-L. Zhang, Z.-Q. Tian, L. Zhang, C. Liu, Y. Lin, et al., Electrochemical tuning of luminescent carbon nanodots: from preparation to luminescence mechanism, Adv. Mater. 23 (2011) 5801–5806.
[23] H. Zheng, Q. Wang, Y. Long, H. Zhang, X. Huang, R. Zhu, Enhancing the luminescence of carbon dots with a reduction pathway, Chem. Commun. 47 (2011) 10650–10652.
[24] G. Eda, Y.-Y. Lin, C. Mattevi, H. Yamaguchi, H.-A. Chen, I.S. Chen, et al., Blue photoluminescence from chemically derived graphene oxide, Adv. Mater. 22 (2010) 505–509.
[25] J. Peng, W. Gao, B.K. Gupta, Z. Liu, R. Romero-Aburto, L. Ge, et al., Graphene quantum dots derived from carbon fibers, Nano Lett. 12 (2012) 844–849.
[26] S. Kim, S.W. Hwang, M.-K. Kim, D.Y. Shin, D.H. Shin, C.O. Kim, et al., Anomalous behaviors of visible luminescence from graphene quantum dots: interplay between size and shape, ACS Nano 6 (2012) 8203–8208.
[27] Y.-Q. Zhang, D.-K. Ma, Y. Zhuang, X. Zhang, W. Chen, L.-L. Hong, et al., One-pot synthesis of N-doped carbon dots with tunable luminescence properties, J. Mater. Chem. 22 (2012) 16714–16718.
[28] J. Zhou, Y. Yang, C.-Y. Zhang, A low-temperature solid-phase method to synthesize highly fluorescent carbon nitride dots with tunable emission, Chem. Commun. 49 (2013) 8605–8607.
[29] S. Qu, X. Wang, Q. Lu, X. Liu, L. Wang, A biocompatible fluorescent ink based on water-soluble luminescent carbon nanodots, Angew. Chem. Int. Ed. 51 (2012) 12215–12218.

[30] H. Peng, Y. Li, C. Jiang, C. Luo, R. Qi, R. Huang, et al., Tuning the properties of luminescent nitrogen-doped carbon dots by reaction precursors, Carbon 100 (2016) 386–394.
[31] J.L. Bredas, A.J. Heeger, Influence of donor and acceptor substituents on the electronic characteristics of poly(paraphenylene vinylene) and poly(-paraphenylene), Chem. Phys. Lett. 217 (1994) 507–512.
[32] F. Babudri, G.M. Farinola, F. Naso, R. Ragni, Fluorinated organic materials for electronic and optoelectronic applications: the role of the fluorine atom, Chem. Commun. (2007) 1003–1022.
[33] F.C. Krebs, H. Spanggaard, An exceptional red shift of emission maxima upon fluorine substitution, J. Org. Chem. 67 (2002) 7185–7192.
[34] H. Zhu, X. Wang, Y. Li, Z. Wang, F. Yang, X. Yang, Microwave synthesis of fluorescent carbon nanoparticles with electrochemiluminescence properties, Chem. Commun. (2009) 5118–5120.
[35] C.S. Castro, M.C. Guerreiro, L.C.A. Oliveira, M. Goncalves, A.S. Anastacio, M. Nazzarro, Iron oxide dispersed over activated carbon: support influence on the oxidation of the model molecule methylene blue, Appl. Catal. A 367 (2009) 53–58.
[36] S. Chen, J.-W. Liu, M.-L. Chen, X.-W. Chen, J.-H. Wang, Unusual emission transformation of graphene quantum dots induced by self-assembled aggregation, Chem. Commun. 48 (2012) 7637–7639.
[37] D.S. English, L.E. Pell, Z.H. Yu, P.F. Barbara, B.A. Korgel, Size tunable visible luminescence from individual organic monolayer stabilized silicon nanocrystal quantum dots, Nano Lett. 2 (2002) 681–685.
[38] L. Wang, S.-J. Zhu, H.-Y. Wang, S.-N. Qu, Y.-L. Zhang, J.-H. Zhang, et al., Common origin of green luminescence in carbon nanodots and graphene quantum dots, ACS Nano 8 (2014) 2541–2547.